MAGNETIC RESONANCE IN MEDICINE

Perfusion Imaging by a Flow-sensitive Alternating Inversion Recovery (FAIR) Technique: Application to Functional Brain Imaging

Seong-Gi Kim, Nikolaos V. Tsekos

Perfusion is a crucial physiological parameter for tissue function. To obtain perfusion-weighted images and consequently to measure cerebral blood flow (CBF), a newly developed flow-sensitive alternating inversion recovery (FAIR) technique was used. Dependency of FAIR signal on inversion times (TI) was examined; signal is predominantly located in large vessels at short TI, whereas it is diffused into gray matter areas at longer TI. CBF of gray matter areas in the human brain is 71 ± 15 SD ml/100 g/min (n = 6). In fMRI studies, micro- and macrovessel inflow contributions can be obtained by adjusting TIs. Signal changes in large vessel areas including the scalp were seen during finger opposition at a TI of 0.4 s; however, these were not observed at a longer TI of 1.4 s. To compare with commonly used BOLD and slice selective inversion recovery techniques, FAIR and BOLD images were acquired at the same time during unilateral finger opposition. Generally, activation sites determined by three techniques are consistent. However, activation of some areas can be detected only by FAIR, not by BOLD, suggesting that the oxygen consumption increase couples with the CBF change completely. Relative and absolute CBF changes in the contralateral motor cortex are 53 ± 17% SD (n = 9) and 27 ± 11 SD ml/100 g/min (n = 9), respectively.

Key words: cerebral blood flow; perfusion; functional magnetic resonance imaging; functional brain mapping.

INTRODUCTION

Adequate rates of blood flow are crucial for proper maintenance of normal metabolic rates in animals and humans. To measure tissue blood flow, two major MR approaches have been developed; one uses *exogenous* tracers, and the other is based on *endogenous* tracers.

The use of *exogenous* tracers includes tracer kinetics and first passage imaging. After an administration of exogenous freely diffusible tracers such as D_2O and perfluorocarbons (1–6), the tracers in the tissue are monitored over time using NMR spectroscopy. Tissue blood flow can be determined from a tracer time course (5). Although this technique has been successfully used in animal studies, it has not been applied to humans because of concerns about the large amounts of tracers required. First-pass imaging has been used after a bolus injection of a paramagnetic agent such as Gd-DTPA. Although cerebral blood flow (CBF) cannot be obtained easily, cerebral blood volume (CBV) can be determined by integrating MRI signals over the first passage of the contrast agent (7). This method was successfully applied to detect CBV changes during visual stimulation (8). However, the use of this technique is severely limited by the need for repeated bolus injections of an exogenous contrast agent to monitor flow changes due to neuronal activities and drugs.

The *endogenous* tracer method using water protons as a contrast agent is classified into two categories; one is to perturb spins outside of an imaging slice, and the other is to perturb spins within the imaging slice. The former includes continuous inversion of the inflowing spins (9–11), and signal targeting with alternating radio frequency (STAR) methods (12). After the arterial blood spins are prepared with inversion or saturation, tagged spins move into capillaries and exchange with tissue water spins. The tagging pulse is applied continuously to the neck area or as a short pulse to the inferior area of the imaging slice. Subsequent to spin tagging (e.g., inversion), the tag is lost by T_1 relaxation whereas spins travel into the imaging slice. The signal difference between images with and without spin tagging is directly related to tissue blood flow. The continuous tagging method was successfully used to measure CBF of animals (9–10). In human studies, the transit time of tagged blood spins is long since they must travel from the carotid artery at the neck to the imaging slice, resulting in significant signal loss of the tagged spins (11). Long pulses for continuous spin tagging create magnetization transfer (MT) effects when a single coil is used for both spin preparation and imaging (13). Although the use of two coils can eliminate MT effects, implementation of such a coil is difficult. The continuous tagging technique can measure absolute blood flow at the steady state condition, but it has not been used for examination of flow changes related to increased mental activity. To detect signal changes induced by brain functional activities, Edelman *et al.* (12) have used the pulsed spin tagging method, echo planar imaging and STAR (EPISTAR), in which two images are acquired with and without spin tagging at the proximal end of the arterial blood and then one is subtracted from the other. Focal signal changes during visual stimulation and finger movements were observed. However, the exact relationship between the percent signal changes in the images and the alterations in CBF is complicated due to the loss of tagged spins during the transit time (12). Furthermore, additional slice-selective saturation pulses before inversion are required to subtract stationary signals from two images.

MRM 37:425–435 (1997)

From the Center for Magnetic Resonance Research, Department of Radiology, University of Minnesota Medical School, Minneapolis, Minnesota.

Address correspondence to: Seong-Gi Kim, CMRR, University of Minnesota Medical School, 385 East River Road, Minneapolis, MN 55455.

Received April 2, 1996; revised August 19, 1996; accepted August 24, 1996.

Supported by National Institutes of Health Grants RR08079, NS32919, and NS32437, and a Grant-in-Aid from the University of Minnesota.

0740-3194/97 $3.00

Perfusion methods which perturb the spins within the imaging slice rely on inflow of the unperturbed longitudinal magnetization (M_0) along the $+z$ direction outside the slice, and thus are independent of the T_1 relaxation of the blood water protons during the transit time. Slice-selective inversion recovery and flow-sensitive alternating inversion recovery (FAIR) methods belong to this category (14–16). The slice-selective inversion recovery (ssIR) technique has been used to map visual stimulation in the brain (14). Absolute CBF at the steady state condition and change of *relative* CBF (relCBF) can not be measured, but index of CBF change can be determined. Since echo planar imaging (EPI) techniques are used for data collection, it is inevitable that T_2* weighting will appear in the IR images (14). Thus, activation based on the IR technique has compounding effects from T_2* as well as from CBF changes. Recently, the FAIR technique has been used to measure relCBF changes (15). Using this technique, perfusion-based functional images can be generated by taking the difference of two IR images, one with a global inversion pulse and another with a slice-selective inversion pulse. The signal changes are directly correlated to CBF changes so that quantification of relCBF changes during mental processes is possible. Since ssIR images are acquired as part of FAIR images, changes of CBF can also be measured (14). The FAIR technique can be used to determine absolute CBF at the steady state condition (15, 16).

In this study, several issues related to the FAIR technique were investigated by theoretical calculation and experiments. Since fMRI images were acquired during a steady state condition, the optimal condition was determined by simulation. Experimentally, CBF contrast dependence on inversion times was examined. Absolute CBF of gray matter in the human brain was determined, and the ratio of CBF between white and gray matter was estimated. In fMRI studies, effects of inversion times were examined by acquiring FAIR images with inversion times of 0.4 and 1.4 s simultaneously. Further, to compare activation sites determined by commonly used blood oxygenation level dependent (BOLD) (17) and ssIR images, FAIR and BOLD images were collected at the same time during unilateral finger opposition. Both absolute and relative CBF changes were determined, in addition to BOLD percent signal changes.

METHODS AND MATERIALS

Technique and Theory

Two IR images are acquired in the FAIR technique; one with a non-slice-selective inversion pulse, and the other with a slice-selective inversion pulse (15). The longitudinal magnetization of tissue-water proton $M(t)$ after an inversion pulse can be described by the Bloch equations,

$$\frac{dM(t)}{dt} = \frac{M_0 - M(t)}{T_1} + fM_a(t) - fM_v(t), \qquad [1]$$

in the presence of flow components, where t is the inversion time, M_0 is the fully relaxed longitudinal magnetization of tissue-water proton, T_1 is the longitudinal relaxation time of tissue-water proton after correcting flow effects, f is the cerebral blood flow (ml/g tissue/s), M_a is the magnetization of arterial blood-water proton, and M_v is the magnetization of venous blood-water proton (9–10). One assumption has been made: blood and tissue water spins exchange instantaneously. Thus, $M_v(t)$ equals $M(t)/\lambda$ where λ is the tissue-to-blood partition coefficient.

Theoretical analysis at a condition of full recovery was described in the previous study (15). However, in practice, experiments will be performed at a steady state. Images with a slice-selective IR pulse ($180°_{ss}$) and a non-slice selective IR pulse ($180°_{ns}$) are acquired alternatively and repeatedly with an inversion time (TI) and a delay time (τ) between excitation and subsequent 180° pulses, i.e., the repetition unit is $180°_{ss}$ - TI- $90°_{ss}$ - τ -$180°_{ns}$ - TI - $90°_{ss}$ - τ, where $90°_{ss}$ is the slice-selective excitation pulse. The repetition time (TR) is defined as the sum of TI and τ.

After the $180°_{ss}$ pulse, $M(0)$ is inverted, whereas $M_a(t)$ outside of the inversion slab is the relaxed longitudinal magnetization. Thus, $M(t)$ recovers with the apparent longitudinal relaxation time (T_1*) which contains an inflow component M_0, i.e., $1/T_1^* = 1/T_1 + f/\lambda$ (9, 10). This assumption is valid when the longitudinal magnetization of the arterial spins is fully relaxed. For example, in saturation recovery used in EPISTAR, inflowing arterial spins are inverted; thus the above equation regarding the apparent relaxation time should be modified. The longitudinal magnetization measured at TI after a $180°_{ss}$ pulse, M_{ss}(TI), is

$$M_{ss}(\mathrm{TI}) = M_0 - 2 \cdot M_0 \cdot e^{-\mathrm{TI}/T_1^*} + M_0 \cdot e^{-\mathrm{TI}/T_1^*} \cdot e^{-\tau/T_1^*} \qquad [2]$$

After the $180°_{ns}$ pulse, $M_a(0)$ and $M(0)$ are inverted. Assuming that both tissue and blood have the same T_1, $M_a(t)$ and $M(t)$ are equivalent. Thus, the relaxation of $M(t)$ is governed by T_1. The longitudinal magnetization M_{ns}(TI) is

$$M_{ns}(\mathrm{TI}) = M_0 - 2 \cdot M_0 \cdot e^{-\mathrm{TI}/T_1} + M_0 \cdot e^{-\mathrm{TI}/T_1} \cdot e^{-\tau/T_1^*} \qquad [3]$$

In the case that $TR > 3 \times T_1$ and $\mathrm{TI} < 0.7 \times T_1$ (i.e., shorter than zero-crossing point), M_{ss} is greater than M_{ns} in magnitude mode, whereas with $\mathrm{TI} < 0.7 \times T_1$, M_{ss} is less than M_{ns}.

When M_{ns}(TI) is subtracted from M_{ss}(TI), the signal difference between two IR images ΔM(TI) is given by

$$\Delta M(\mathrm{TI}) = M_0 \cdot e^{-\mathrm{TI}/T_1} \cdot (1 - e^{-\mathrm{TI} \cdot f/\lambda}) \cdot (2 - e^{-\tau/T_1^*}). \qquad [4]$$

Expanding the exponential term with f of 0.01 ml/g tissue/s and λ of 0.9 ml/g (18), and ignoring a quadratic flow term, Eq. [4] can be rewritten as

$$S_{\mathrm{FAIR}} = \frac{f}{\lambda} \cdot \mathrm{TI} \cdot M_0 \cdot (2 \cdot e^{-\mathrm{TI}/T_1} - e^{-\mathrm{TR}/T_1}), \qquad [5]$$

where S_{FAIR} is the signal intensity of the subtraction FAIR image. Eq. [5] demonstrates that, by measuring T_1 and M_0 from T_1-weighted images with non-slice selective inversion, absolute CBF can be determined from FAIR images.

In functional activation studies, FAIR images are acquired during both control and stimulation periods. Then, difference images during the control period $S_{FAIR(cont)}$ and task period $S_{FAIR(st)}$ are calculated. These signal changes during the task period can be described as

$$\frac{\Delta S_{FAIR}}{S_{FAIR(cont)}} = \frac{S_{FAIR(st)}}{S_{FAIR(cont)}} - 1 = \frac{f_{st}}{f_{cont}} - 1 \qquad [6]$$

where f_{st} and f_{cont} are the CBF during task and control periods, respectively.

Since ssIR images are also acquired in the FAIR technique, absolute CBF changes can be determined. In the steady state condition (14), the longitudinal magnetization M is dependent on TI and TR, as shown in Eq. [2]. The task-induced signal change of ssIR images is described as (14)

$$\frac{\Delta M}{M} = \frac{2 \cdot \mathrm{TI} \cdot e^{-\mathrm{TI}/T_1} - TR \cdot e^{-TR/T_1}}{1 - 2e^{-\mathrm{TI}/T_1} + e^{-TR/T_1}} \Delta\left(\frac{f}{\lambda}\right), \qquad [7]$$

Here, T_1 is defined as the apparent longitudinal relaxation time during the control period, which is the same as T_1* during the control period shown in Eq. [2].

Due to the use of EPI data collection in this study, it is inevitable that there will be a T_2* contribution as well as T_1 relaxation in the IR images. From the FAIR and BOLD signal changes, only the flow component can be extracted as relCBF = [(1 + fractional change of FAIR)/(1 + fractional change of BOLD) − 1]. A detailed analysis was described in the preliminary report (15). Similarly, BOLD effects in ssIR images can be separated. The fractional signal change in ssIR images due only to inflow effects equals [(1 + fractional change of ssIR)/(1 + fractional change of BOLD) − 1].

Computer Simulation

To determine the effect of various parameters in the FAIR sequence, S_{FAIR} was simulated by varying TI and τ values, and then normalized by a repetition time (TR). To calculate Eqs. [2] and [3], an f value of 0.01 ml/g tissue/s and λ of 0.9 were used. The normalized intensity $S_{FAIR(norm)}$ is described as $S_{FAIR(norm)} = S_{FAIR}/TR^{1/2}$. Relative CBF change can be determined by using Eq. [6]. To determine errors in the relCBF calculation due to the expansion of exponential terms, the relCBF changes determined by Eq. [6] were compared with actual relCBF changes.

MRI during a Steady State Condition

Normal human subjects were studied on a 4T whole body imaging system with a 1.25 m diameter horizontal bore (SIS Co., Palo Alto, CA/Siemens, Erlangen, Germany) and a head gradient insert operating at a gradient strength of 30 mT/m and a slew rate of 150 T/m/s in all three axes. For RF transmission and detection, a homogeneous quadrature birdcage coil was used (19). Manual shimming was performed to improve homogeneity before the image data collection.

In all imaging studies, conventional anatomic images were collected using a TurboFLASH technique with slice-selective inversion to identify large inflow areas. Typical imaging parameters were a TI of 1.2 s, a TE of 4.7 ms, a TR of 9.6 ms, an in-plane resolution of 0.94 × 0.94 mm^2, and a slice thickness of 5 mm. In addition, T_1-weighted EPI images were acquired using an interleaved EPI technique (20). The parameters were a TE of 8 ms and an in-plane resolution of 1.88 × 1.88 mm^2. To identify large venous vessels, high resolution T_2*-weighted images were acquired using a FLASH technique. Typical parameters were a TE of 13.4 ms and a TR of 22 ms. Since misregistration between conventional and EPI image exists, the exact locations of vessels in EPI images cannot be identified accurately from vessel- and T_1-weighted conventional images. However, gray and white matter areas in EPI can be easily determined from T_1-weighted EPI images.

The FAIR scheme was implemented with two IR images with and without slice-selective gradients during an inversion pulse in an interleaved fashion. The inversion pulses were hyperbolic secant pulses with a pulse length of 8 ms. After an inversion pulse and a delay (i.e., inversion time), EPI images were acquired with trapezoidal gradient shapes for the readout and blipped gradients for the phase-encoding direction. An axial single-shot EPI image had a 64 × 64 matrix size over a field of view of 24 × 24 cm^2 with 5-mm slice thickness. The gradient echo time was set to 20 ms and the acquisition time was 30 ms. Thickness of the slice-selective inversion slab was 15 mm and the centers of both imaging and inversion slices were positioned at the same location. A five-lobe sinc-shaped RF pulse with a pulse length of 4 ms was used for the excitation of spins. All FAIR images were generated by pairwise subtraction of magnitude images with ssIR and nsIR. To obtain CBF contrast, FAIR images were acquired with four inversion times, 0.4, 0.7, 1.2, and 1.6 s. A delay time, τ, after data collection was 5 s and 40 FAIR images were averaged.

Functional MRI during Finger Opposition

A functional imaging slice was selected axially through the finger area in the precentral gyrus. In all studies, the time between an excitation pulse for data collection and subsequent pulse (i.e., τ) was 1.4 s. For fMRI studies, image sets were collected repeatedly during resting "nonstimulated" and "task" periods. Usually, 10 image sets were acquired during each period. The task was visually instructed finger opposition between the thumb and the remaining four digits. Frequency of visual instruction for the finger movement was 1.25 Hz. During the control periods, the identical presentation was displayed to minimize abrupt head movements between periods and as a control for vision and eye movements.

To investigate the effects of TI on the FAIR fMRI images, two inversion times of 0.4 and 1.4 s were used in an alternative manner. The order of data collection for each image set was slice-selective IR (ssIR) with a TI of 1.4 s, ssIR with a TI of 0.4 s, non-slice selective IR (nsIR) with a TI of 1.4 s, and nsIR image with a TI of 0.4 s. FAIR images with TI of 0.4 s were obtained by subtraction of

ssIR from nsIR images; those with TI of 1.4 s were determined by subtraction of nsIR from ssIR images. The flip angle of excitation pulses was 90°.

To compare BOLD-, IR-, and FAIR-based functional maps, IR and BOLD images were acquired in an interleaved fashion. EPI image sets were acquired in the following order: ssIR with a TI of 1.4 s, BOLD with a *TE* of 20 ms (BOLD20), nsIR with a TI of 1.4 s, and BOLD image with a *TE* of 30 ms (BOLD30). The flip angles for excitation were 90° and 45° for IR and BOLD images, respectively.

From the consecutive images generated during the paradigm, functional maps were calculated according to two criteria: (i) The cross-correlation method was used with a boxcar reference waveform (21); only pixels with statistically significant activation ($P < 0.05$) were included. A cross-correlation value was chosen based on the number of images used (21). (ii) Regions with less than 4 contiguous activated pixels were not included in the functional map (22). Percent signal changes were also calculated by the averaged signal difference of the activated pixels between control and task periods divided by the averaged signal intensity of the same pixels during the control period.

Relative and absolute CBF changes caused by finger opposition were calculated. Because the gradient-echo EPI technique was used for data collection, BOLD effects were separated from IR images using BOLD20 images. To determine absolute CBF changes, Eq. [7] can be used. However, in our cases, because a 45° flip angle for BOLD images was used before IR images, Eq. [7] needs to be modified as follows:

$$\frac{\Delta M}{M} = \frac{2 \cdot \mathrm{TI} \cdot e^{-\mathrm{TI}/T_1} - (1 - \cos\alpha) \cdot TR \cdot e^{-TR/T_1} - \cos\alpha \cdot (TR + \tau) \cdot e^{-(TR+\tau)/T_1}}{1 - 2e^{-\mathrm{TI}/T_1} + (1 - \cos\alpha)\, e^{-TR/T_1} + \cos\alpha \cdot e^{-(TR+\tau)/T_1}} \cdot \frac{f}{\lambda}\Delta(\cdot). \quad [8]$$

where TR is the repetition time of the IR images (2.8 s), τ is the delay between IR excitation and BOLD excitation pulses (1.4 s), and α is the flip angle of BOLD images (45°). In the case that $\alpha = 90°$, Eq. [8] is the same as Eq. [7].

RESULTS

Computer Simulation

Although the exact condition for the maximal SNR depends on τ and TI, maximum S_{FAIR} is achieved at TI $\approx T_1$ and τ ranging from $0.5 \times T_1$ to T_1. In all fMRI studies, τ was set to 1.4 s, which is the T_1 of gray matter water protons at 4 Tesla (23). Also, the TI was set to 1.4 s, except for the inversion time dependency studies. Higher CBF changes and longer τ values resulted in higher errors due to the expansion of the exponential terms. The relCBF change induced by neuronal activity is expected to be less than 300%, which caused a fractional error of <3%. This error was much less than SNR of FAIR images. Thus, we did not attempt to correct the errors in relCBF data.

CBF Contrast at Different Inversion Times

Figure 1 shows anatomic and FAIR images. The slice position is shown in (A); the imaging slice of 5-mm thickness (the inner box) was oriented axially, and the thickness of the slice-selective inversion slab (the outer box) was 15 mm. The high resolution (256 × 256) T_1-weighted image (B) has gray/white matter contrast and also signal enhancement in large vessel areas which appear as bright lines. The FAIR images (i.e., subtraction images) with a TI of 0.4 and 0.7 s were calculated by subtraction of the ssIR image from the corresponding nsIR image, whereas those with a TI of 1.2 and 1.6 s were determined by subtraction of the nsIR image from the

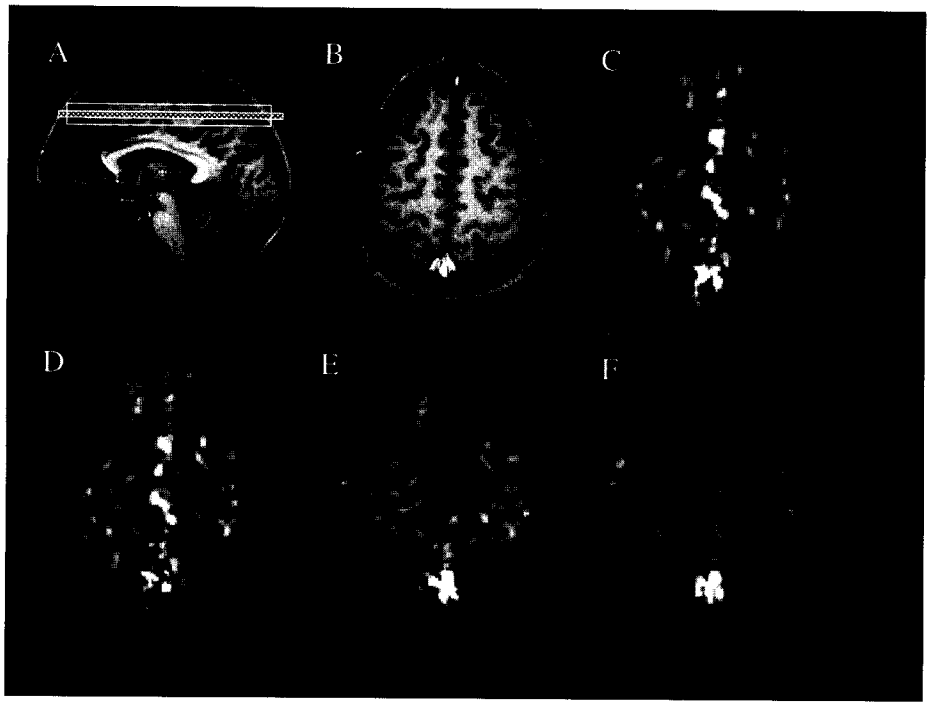

FIG. 1. FAIR images at different inversion times. (A) shows the slice-selection for FAIR images. The inner box represents the imaging slice with 5-mm thickness and the outer box represents the slice-selective inversion slab with 15-mm thickness. (B) represents a high resolution T_1-weighted anatomic image (TI = 1.2 s, *TE* = 5 ms, and *TR* = 10 ms). Areas with high signal intensities are due to large inflow effects, indicating large vessels, The FAIR images with inversion times of 0.4, 0.7, 1.2, and 1.6 s are shown in (C), (D), (E), and (F), respectively. Top of the FAIR images is anterior.

ssIR image. Positive signal intensity is displayed using a gray scale in FAIR images, whereas negative signal intensity is shown as black. The image intensities of four FAIR images are consistent with theoretical expectations: $M_{ss} < M_{ns}$ when TI $< 0.7 \cdot T_1$, whereas $M_{ss} > M_{ns}$ when TI $> 0.7 \cdot T_1$ in the magnitude mode. In the FAIR image with a TI of 0.4 s, (C), signal enhancement was predominantly located at large vessel areas, which were correlated with areas of high signal intensities in the anatomic image. When the inversion time increased, smaller signal enhancement was present in the diffused gray matter areas. The FAIR image with a TI of 1.6 s, (F), has excellent contrast between white and gray matter; the gray matter areas have high signal intensities, whereas the white matter areas have low signal intensities. The average signal intensity ratio of gray and white matter was 3.5. The signal intensities in large vessel areas including the sagittal sinus are the highest at TI of 0.4–0.7 s, whereas those in gray matter and white matter areas are the highest at TI of 1.2–1.6 s. Dependency of signal changes in white matter areas on inversion times cannot be seen here due to poor reproduction of images.

TI Dependency

The FAIR technique, similar as ssIR and EPISTAR techniques, can separate macro- and microvascular flow effects by using different TIs. Fig. 2 shows FAIR images with a TI of 0.4 and 1.4 s and their functional statistical maps during left hand finger opposition (subject 21). Since images were acquired alternatively during the same task, the physiological conditions were identical in both images. In the FAIR image with a TI of 0.4 s (Fig. 2A), signal enhancement was predominantly located in the large vessel areas, which were easily identified in the high resolution T_1-weighted image. When the TI was increased to 1.4 s (Fig. 2C), signal enhancement was observed in gray matter areas, also seen in Fig. 1. During left hand finger opposition, the signal intensity of the right motor area (anterior to the central sulcus indicated by the arrow) increased in the functional map with a TI of 0.4 s (Fig. 2B). In addition, signal changes were observed in large vessel areas, including the scalp. However, most of the pixels which showed signal changes at TI = 0.4 s did not exhibit signal changes at TI = 1.4 s. Since large vessels are completely replenished with tagged spins during TI 1.4 s, velocity increases can not cause any intensity changes. Importantly, activation areas were mainly located in the gray matter areas, including the right primary motor and bilateral premotor areas. Small, but significant, activation was observed in the ipsilateral (left) motor area. This observation is consistent with our previous studies (24, 25).

Six fMRI experiments were performed by four subjects. The number of pixels activated in the contralateral motor cortical area and percentage signal changes are listed in Table 1. In all experiments, activation of the contralateral motor cortex was found during unilateral finger opposition. Functional activation of all subjects had similar

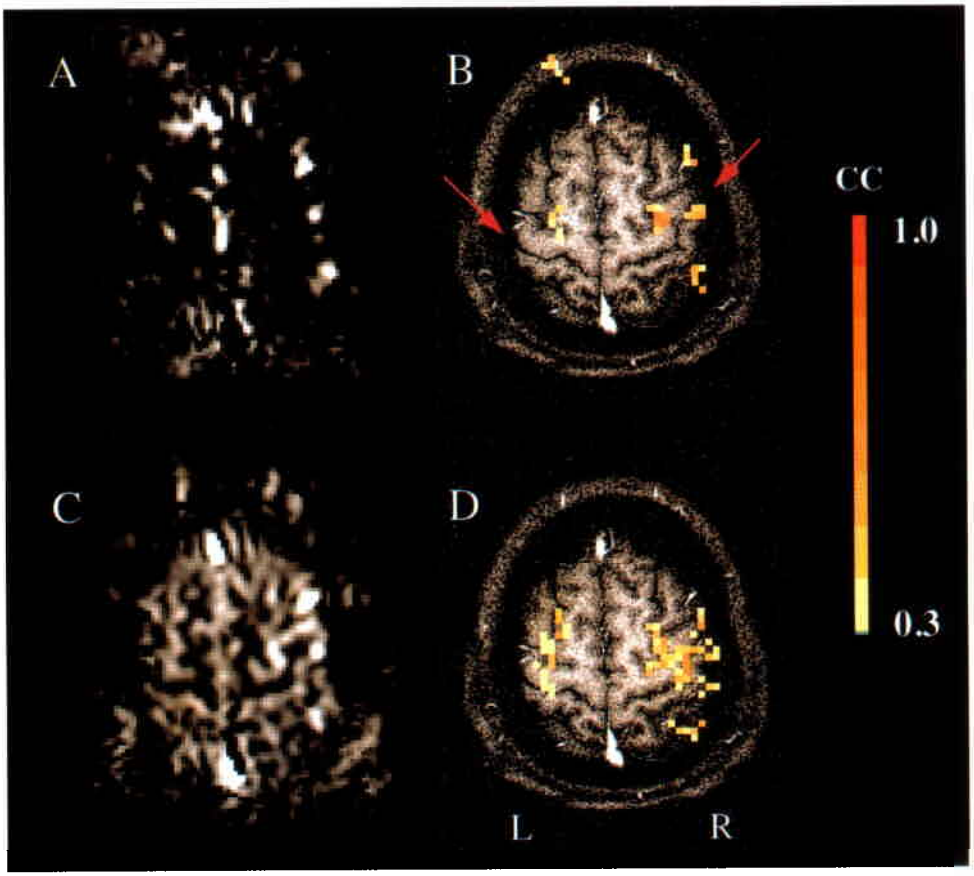

FIG. 2. FAIR images (A) and (C) and functional statistical maps (B) and (D) during left hand finger opposition. Two inversion times of 0.4 (A) and (B) and 1.4 s (C) and (D) were used. The red arrows indicate the central sulcus. In the functional maps, the cross correlation value of 0.3 was used for a threshold. Each color increment represents 0.1 increase of a cross correlation value in a color bar. R is the right hemisphere and L is the left hemisphere.

Table 1
Number of Activated Pixels in the Contralateral Motor Area and Their Percent Changes in Parentheses

Subject[a]	0.4 s FAIR[b]	1.4 s FAIR[c]	Ratio[d]
1r	6 (342)	20 (48.7)	3.3 (0.14)
1l	5 (214)	15 (45.7)	3.0 (0.21)
2l	12 (147)	34 (49.6)	2.8 (0.33)
3r	10 (212)	13 (39.2)	1.3 (0.18)
3l	4 (521)	13 (126)	3.3 (0.24)
4l	9 (95.6)	11 (67)	1.2 (0.70)
Mean ± SD	7.7 ± 3.1 (255 ± 154)	17.7 ± 8.6 (62.7 ± 32.4)	2.1 ± 4.2 (0.2 ± 0.5)

[a] Two subjects performed right (r) and left hand (l) finger opposition and two other subjects performed only left hand finger opposition.
[b] FAIR images were acquired with a TI of 0.4 s.
[c] FAIR images were acquired with a TI of 1.4 s.
[d] Ratio was calculated by the FAIR with a TI of 1.4 s divided by the FAIR with 0.4 s.

patterns, as seen in Fig. 2. The activated area found with a TI of 1.4 s was larger than that found with a TI of 0.4 s. More importantly, sites of signal changes found with a TI of 0.4 s were located mainly at the central sulcus, whereas those found with a TI of 1.4 s were chiefly in tissue areas. Percent signal change with a TI of 0.4 s was about 5 times higher than that with a TI of 1.4 s.

FAIR *versus* IR *versus* BOLD Images

To compare FAIR, IR, and BOLD images, both IR and T_2*-weighted EPI images were acquired alternatively. Data sets from six subjects were used to determine signal intensities and fluctuations. Based on FAIR and T_1-weighted EPI images, gray matter areas were selected. Signal intensity of images with *TE* of 30 ms was 0.81 ± 0.01 SD (n = 6) of the corresponding image intensity with a *TE* of 20 ms, yielding a T_2* of gray matter equal to 45 ms. This was consistent across subjects. Signal intensity of FAIR images within gray matter was 2.8 ± 0.6% SD (n = 6), ranging from 2.2 to 3.8% of the corresponding 20 ms T_2*-weighted BOLD image intensity. Note that flip angles were 45° for BOLD experiments and 90° for the FAIR studies.

With the FAIR signal intensity, absolute CBF can be determined using Eq. [5]. During a steady state condition, the signal intensity of the BOLD image after a τ delay after a 90° pulse equals $[1 - \exp(-\tau/T_1^*)] \cdot \cos(\alpha) \cdot M_0$ where τ = 1.4, T_1^* = ~1.4, and α = 45°. When flip angles were taken into account, FAIR intensity within gray matter, ΔM, was 1.3 ± 0.3% SD (n = 6) of the full relaxed longitudinal magnetization. With the known value λ of 0.9 (20), T_1 of 1.4 s (23), and TI of 1.4 s, CBF of the gray matter areas was determined to yield 81 ± 17 SD ml/100 g tissue/min (n = 6), ranging between 63 and 109 ml/100 g/min. In Eq. [5], it is assumed that an inversion pulse follows a 90° pulse. Since a pulse with 45° flip angle was used before an inversion pulse, the calculated CBF was over-estimated by 10%. The actual CBF was 71 ± 15 ml/100 g/min in the gray matter area (the average age was 29 ± 6.6 SD years, n = 6).

An important parameter in fMRI is the task-induced signal change to signal fluctuation ratio ("contrast-to-noise ratio; " CNR) because functional maps are calculated using statistical tests. Task-induced signal changes were determined from activated pixels within the contralateral motor cortex. Only images acquired during the control period were used to calculate fluctuations of signals as standard deviations in gray matter areas, devoid of large vessels. CNRs of BOLD20, BOLD30, ssIR, and FAIR were 1.72 ± 0.82, 1.67 ± 0.78, 1.20 ± 0.45, and 0.77 ± 0.18 SD (n = 6), respectively. BOLD images with both 20 and 30 ms TEs have higher CNRs than both FAIR and IR images. In the BOLD images, signal changes from large venous vessels may contribute significantly, resulting in overestimation of CNR.

FAIR *versus* IR *versus* BOLD Functional Maps during Finger Opposition

Figure 3 shows results of a representative functional study (subject 6l) during left hand finger opposition. Percent signal changes generated from BOLD30, IR, and FAIR images (Figs. 3A, 3B, and 3C, respectively) were calculated in pixels which were statistically significant (i.e., a cross correlation value of 0.3). In the T_1-weighted image with slice-selective inversion (Fig. 3D), large signal intensities were clearly seen at the right central sulcus (shown as a red arrow) due to large inflow effects into the imaging slice. In the high resolution T_2*-weighted image (Fig. 3E), dark lines were observed due to short T_2* of deoxyhemoglobin in large venous vessels, and bright areas were seen due to the long T_2* of cerebrospinal fluid. A composite map (Fig. 3F) was generated by both BOLD30 and FAIR maps.

Careful inspections revealed several observations. (i) Generally, activation sites are compatible in all three fMRI maps; signal changes were observed at the right motor cortex (see also Fig. 3F). As expected from the CNR, BOLD- and IR-based maps have a larger activation area in the right motor cortex than the FAIR-based map. (ii) In the BOLD30 map, the left (ipsilateral) supplementary motor area (SMA) in the middle of the image (shown a circle in Fig. 3D) was activated, whereas the right (contralateral) SMA showed activation in the FAIR map. However, in the IR map, the bilateral SMA as well as the ipsilateral motor cortex were activated. When the threshold value of both BOLD and FAIR images was decreased to a cross-correlation value of 0.2, activation of the bilateral SMA was observed in both maps. (iii) Additional activation sites of the right motor cortex seen only in the FAIR map were located in the middle between the midline and the right edge of the brain (see also green pixels in Fig. 3F). Even though the cross-correlation value was decreased to 0.2, these pixels were not activated in BOLD and IR maps. (iv) In the BOLD- and IR-based functional images, additional signal changes were observed in the anterior side of the brain due to flow artifacts. These artifacts were subtracted in the FAIR image and thus no signal changes were observed. (v) Higher signal changes were seen in IR- than in BOLD-based maps since both flow and BOLD components contributed to IR images. In the BOLD image, 1–2% signal changes were detected in tissue areas within the right motor cortex, whereas signal changes greater than 10% were observed in the right central sulcus (see also Fig. 3F). Contrary, ca. 100% CBF changes were seen in the tissue, whereas CBF

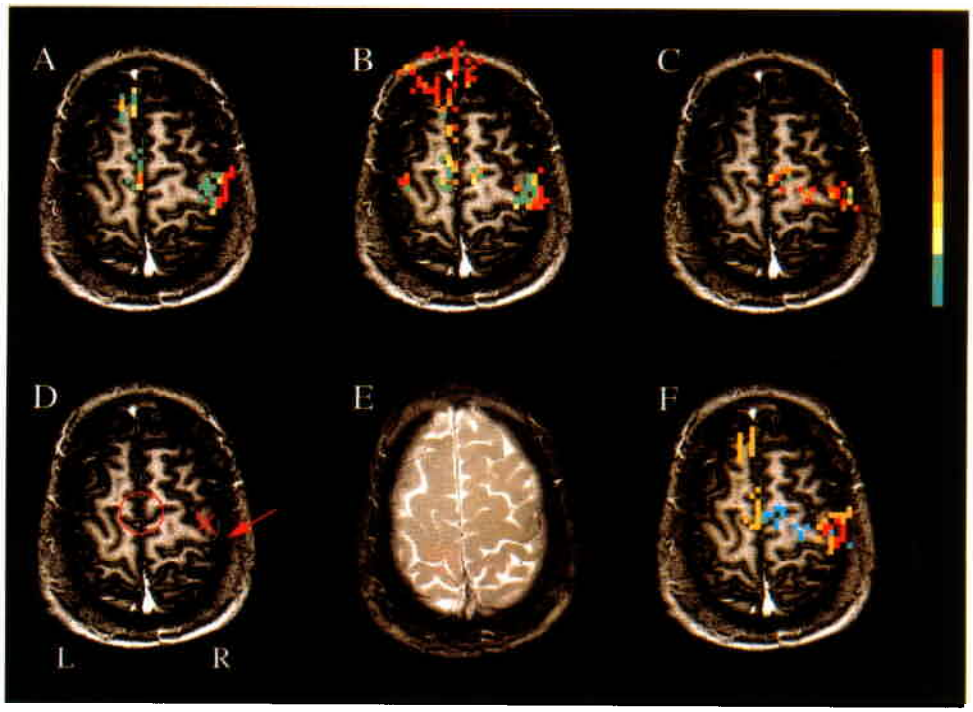

FIG. 3. Functional imaging studies of a subject during left hand opposition. (A), (B), and (C) represent percent change maps of 30-ms BOLD, slice selective IR and FAIR on an anatomic image, respectively. The cross correlation value of 0.3 was used for a threshold. For BOLD and ssIR images, each color represents a 1% increment starting from the bottom 1%, whereas for the FAIR image, percent change at each color increases 10% starting from 10%. (D) and (E) are high resolution T_1- and T_2'-weighted images, respectively. (F) represents a composite map from 30 ms BOLD and FAIR maps: red, commonly activated area; blue, activated area only by FAIR; and yellow, activated area only by BOLD. R, the right hemisphere; L, the left hemisphere; arrow in (D), the central sulcus; circle in D, the supplementary motor area; and · in (D), tissue area. Top of images is anterior.

changes less than 50% were found at the sulcus. In the tissue area shown as × in Fig. 3D, FAIR and BOLD changes were 88 and 1.8% respectively. Large BOLD, but small CBF changes, were located at or nearby large venous vessels. Note that a slight misregistration between conventional anatomic images and EPI-based fMRI is seen in the Rolandic vein, but tissue areas can be easily identified by additional comparison with T_1-weighted EPI images.

Nine experiments were performed by six subjects. The number of activated pixels within the contralateral motor cortex and average signal changes of activated pixels are listed individually in Table 2. Major activation sites were consistent across techniques. The number of activated pixels was similar in BOLD images with TEs of 20 and 30 ms and ssIR images since the CNRs of these images were similar. As expected, the number of activated pixels in the FAIR maps were less than that of other maps. However, since BOLD and IR images may contain contributions from large *venous* vessels, actual activated pixels within gray matter areas may be less. The signal change in the ssIR image only due to CBF effects was 1.3 · 0.5% SD (n 9), ranging from 0.5 to 2.2%. The CBF change in the contralateral motor cortex was 27 · 11 SD ml/100 g/min (n 9), ranging from 10 to 45 ml/100 g/min and the relCBF change in the contralateral motor cortex was 53 · 17% SD (n 9), ranging between 36 and 86%.

Table 2
Number of Pixels Activated in the Contralateral Motor Area and Their Percent Signal Changes in Parentheses

Subject	BOLD20	BOLD30	FAIR	ssIR
5r	23 (3.4)	30 (4.1)	5 (42)	17 (5.7)
5l	32 (8.9)	32 (8.4)	19 (54)	31 (10.5)
6r	27 (3.4)	21 (4.3)	8 (93)	25 (4.2)
6l	14 (3.1)	15 (3.7)	12 (75)	17 (3.6)
7r	42 (1.6)	43 (2.1)	11 (38)	35 (3.0)
7l	19 (1.8)	18 (1.9)	3 (61)	28 (3.3)
8r	39 (3.2)	33 (3.3)	23 (50)	41 (4.5)
9l	20 (2.3)	24 (2.5)	15 (58)	35 (3.3)
10r	71 (1.8)	56 (2.5)	26 (49)	51 (3.6)
Mean · SD	32 · 17 (3.3 · 2.2)	30 · 13 (3.6 · 2.0)	14 · 8 (58 · 17)	31 · 11 (4.6 · 2.3)

DISCUSSION

Qualitative and Quantitative Perfusion Measurements during a Steady State Condition.

A FAIR image with a long inversion time (e.g., 1.6 s) provides excellent perfusion contrast. The ratio of signal intensities in gray and white matter, 3.5, is related to differences of the CBF as well as T_1, as shown in Eq. [5] with a fully relaxed condition (no TR term). We assumed that spin density is the same in both tissue types. The T_1 contribution will be 1.5 times greater in the gray matter

than in the white matter since the T_1s of gray and white matter areas are approximately 1.4 and 0.9 s (23), respectively. Therefore, the residual signal difference of 2.3 is due to the CBF difference between gray and white matter areas; gray matter has a higher CBF than white matter. This observation agrees with reported ratios of gray and white matter, e.g., 2.1 in Pantano *et al.* (26) and 3.4 in Lenzi *et al.* (27).

The CBF can be determined using Eq. [5] with determinations of S_{FAIR}, T_1 and M_0. Only a single FAIR image is needed. In FAIR versus BOLD studies, M_0 can be estimated from the BOLD image with the same echo time (20 ms) and thus the CBF can be determined. The CBF of gray matter determined by FAIR, 71 ± 15 SD ml/100 g/min ($n = 6$), agrees with values determined by positron emission tomography (PET), 73 ± 21 ($n = 16$) (27) and 51 ± 11 SD ml/100g/min ($n = 18$) (26). With a higher SNR, CBF can be determined on a pixel-by-pixel basis.

Absolute cerebral blood flow can be also calculated with T_1 and T_1* (see Technique and Theory section) (9, 10, 16). In the FAIR technique, both T_1 and T_1* can be determined by fitting IR images over inversion times. However, we did not attempt to quantify CBF using this method because of poor SNR, which can be eased by signal averaging, and signal contributions from large vessels. Although we assumed that there is rapid equilibrium of water concentration between the vascular and extravascular spaces of the brain, plug flow from large vessels is a dominant effect for signal changes at short inversion times, which makes it difficult to quantify the CBF. This large vessel contribution can be eliminated using a spin echo sequence with bipolar gradients (28). The signals from stationary tissues refocus at spin echo time, whereas flow components tend to lose signal intensity.

Arterial tagging techniques including FAIR require subtraction of images. DC offset in signal intensities between two images will leave residual signals after subtraction, causing errors in quantification of CBF. To examine whether residual signals exist or not, poorly perfused areas such as scalp muscle can be used as an indicator. To minimize this potential problem due to the imperfect edge effect of inversion pulses, the slice-selective inversion slab should be thicker (three times in this study) than the imaging slice.

We assumed that the T_1 of blood water is the same as the T_1 of tissue water. Although blood T_1 does not contribute to the slice-selective IR images, in the non-slice selective IR images the effective $1/T_1$ will be ρ/T_1 (blood) + $(1 - \rho)/T_1$ (tissue) where ρ is the blood volume fraction. The errors due to different T_1 values were discussed extensively by Kwong *et al.* (16). The T_1 of blood water (~1.5 s) is similar to the T_1 of gray matter (1.4 s), but different from the T_1 of white matter (0.9 s). The CBF in the gray matter areas has little errors, whereas the CBF in the white matter areas is overestimated. Thus, in this study, the errors due to different T_1 values were not corrected in the determination of the CBF in the gray matter area.

We assumed that the feeding flow direction is perpendicular to the imaging plane. In the case where inflow comes from within the slice, the CBF measured by endogenous techniques including FAIR may be underestimated. Thus, slice position and orientation should be chosen carefully. Further, the imaging time for a single slice is on the order of seconds, and thus a large number of slices covering most of the brain can not be easily imaged. This problem exists in all T_1-based techniques.

To deliver tagged water spins into the blood arterial system of the imaging slice, the plug flow velocity of large arterial vessels is important. Typically, arterial blood velocity is 10 cm/s (28) and the distance between edges of the slice-selective inversion slab and excitation slice is less than 1 cm. Thus, it takes approximately 100 ms for tagged spins to enter into the arterial system. Since human rCBF is approximately 60 ml/100 g/min through an intraarterial volume fraction of 0.6% (29), the longest time a spin spends in the arterial system is 600 ms. Altogether it takes less than 700 ms for a tagged spin to transit from the large artery into the capillary system of the imaging slice. Therefore, a TI of greater than 0.7 s should be chosen to have enough time to deliver tagged spins into the imaging slab.

Assuming instantaneous spin delivery to the imaging slice, the SNR of continuous inversion is 2.7 times ($1/e^{-1}$) greater than that of the FAIR with a TI of T_1 (see Technique and Theory section and also ref. 10). In practice, with a single coil system, the SNR of continuous inversion decreased by about 70% due to the MT effect (31). The travel distance of tagged spins should also be considered. For example, in motor experiments, the distance between the neck and the imaging slab is longer than 10 cm for the continuous inversion method (11), whereas in FAIR the travel distance of tagged spins is less than 1 cm. Thus, the continuous inversion time should be much longer than the inversion time in FAIR to maintain the same tagging. However, this is not reasonable in humans because of high power depositions from long RF pulses, especially at high magnetic fields. Furthermore, inverted spins will relax during the travel time (9–12). Considering spin relaxation during delivery and magnetization transfer, the effective SNR of FAIR may be better than that of the continuous inversion.

Separation of Macro- and Microvascular Contributions in FAIR-based fMRI

In fMRI, macrovascular-based functional images do not necessarily correspond with the functionally activated areas (32–37). Thus, it is important to distinguish the macro- *versus* microvascular "inflow" effects in BOLD- and CBF-based fMRI. The *microvasculature* is comprised of capillaries, arterioles, and venules, which coexist in the parenchyma and cannot be distinguished by MR resolution. The *macrovasculature* consists of arteries and veins, which can be identified by high resolution vessel-weighted images. In FAIR images, large vessel contributions were successfully separated from small vessel contributions by varying the inversion times.

The percent signal change at a TI of 0.4 s was much higher than that at a TI of 1.4 s. At a short TI, the vessel areas were not completely refreshed by tagged spins. The degree of refreshment in the imaging slice increased during the performance of tasks due to the macrovascular

velocity increase. This resulted in an apparent "activation," with a high percentage change, that is remote from the actual site of neuronal activity in large vessels such as in the sagittal sinus region. In contrast, the signal change in the FAIR image with a TI of 1.4 s will provide changes of microvascular/perfusion effects. The relCBF changes of all studies except one were similar. The FAIR signal change, 63 ± 32% SD, during finger opposition agrees with previous FAIR data during performance of similar tasks, 48 ± 14% SD (n = 5) (15). Some commonly activated pixels in both maps have high percentage changes in the images with a TI of 0.4 s and low percentage changes in the fMRI with a TI of 1.4 s. These pixels may contain large vessels in part and thus their FAIR signal intensities are predominantly from large vessels. When the signal change is due to a velocity change of plug flow at a short TI, a large percentage change can be obtained. However, at a long TI, signal change is not due to a velocity change of plug flow. Rather it is due to a change of tissue perfusion. In this case, the relCBF change is under-estimated because the high signal intensity from vessels is maintained during both control and task periods.

Relative and Absolute CBF Changes during Performance of Finger Movements

The relCBF change in the contralateral motor cortex was 53 ± 17% SD (n = 9), which is consistent with previous reports during similar movements measured by PET (38–41), and also with the value shown in Table 1 (63 ± 32% without the BOLD correction, n = 6) and our previous report (48 ± 14% SD, n = 5) (15). The CBF change using Eq. [8] was 27 ± 11 SD ml/100 g/min (n = 9). From absolute and relative rCBF changes, rCBF during the control period can be estimated; average CBF during control periods was 51 ml/100 g/min, which is less than the value, 71 ml/100 g/min, determined independently using Eq. [5]. The discrepancy may be related to overestimation of BOLD effects in BOLD20 images, resulting in the underestimation of inflow effects in ssIR images. It is expected that the percent signal changes of BOLD images are linearly dependent on the gradient echo time. However, the ratio of percent signal changes in BOLD images with 20 and 30 ms TEs was less than the expected value of 1.5. This suggests that, although a *TR* of 1.4 s was used, BOLD20 images may contain significant inflow effects.

Comparison of FAIR, BOLD, and IR Methods

Signal fluctuations in a FAIR image may be related to physiological motions. Since the inflow component is the main interest in the CBF experiments, the cardiac pulsation will be problematic for vessel areas, resulting in flow-related large fluctuations. To reduce these problems, gating the inversion pulse to cardiac pulsation may be needed for collecting data during the diastole period, which has the least motion. To compare the CNRs of BOLD and FAIR techniques without large vessel contributions, spin echo-based techniques may be employed. In fMRI studies, averaging is used to improve the SNR. Since BOLD images can be acquired faster, especially in the multi-slice imaging, than IR and FAIR images, the BOLD technique has the highest CNR. However, the BOLD technique is also sensitive to artifacts including slight head motions. In FAIR, slow changes can be corrected by subtraction of an image from its neighbor image. Therefore, the FAIR technique provides clean activation maps even if a lower threshold is applied.

Comparison between fMRI maps using BOLD and FAIR is important because of two reasons: vascular consideration, and the underlying mechanism of BOLD. The BOLD-based functional images have signal changes in veins and presumably capillaries and venules, whereas FAIR-based fMRI images with long tagging times have signal changes predominantly in arterioles and capillaries. When both images are based on the same vascular effects, the microvascular-based activation sites of the two techniques should be spatially identical at the resolution of the MR images, provided that uncoupling between CBF and oxygen consumption (OC) exists. Assuming uncoupling in all areas, areas determined by FAIR (with CBF increase) should be detected by the BOLD technique since CNR of BOLD is greater than that of FAIR. Because its CNR is higher than the CNR of FAIR, BOLD has larger activation areas when the same threshold is applied. The FAIR functional maps with a lower threshold are comparable to the BOLD maps with a higher threshold. When cross-correlation values were adjusted to 0.3 for FAIR and 0.4 for BOLD images, similar activation areas in the motor area were observed, suggesting that both techniques are primarily based on similar vascular effects. It should be noted that, in the spatial resolution of BOLD images used here, BOLD effects from large vessels may not be of concern because these seem to be relatively closely associated with areas of tissue activation, probably due to downstream dilution from vessels draining regions which are not activated by the task (32, 34).

In BOLD images, only areas with the presence of *uncoupling* between CBF and OC during increased neuronal activity can be detected (42). Most activated areas determined by FAIR were also activated in BOLD, indicating these pixels have uncoupling between CBF increase and OC change. However, this may not be present under all circumstances and in all regions of the brain (43, 44). In some subjects, the FAIR technique provides additional activated areas which were not detected by BOLD, as seen in Fig. 3. This suggests that, in these areas, the CBF increase may couple with the OC change completely.

CONCLUSION

A FAIR imaging technique based on IR images and subtraction has been successfully applied to obtain CBF-contrast of the human brain and to measure the relative and absolute blood flow changes during tasking. At long inversion times, excellent perfusion contrast can be obtained. The FAIR technique can separate the large and small vessel contributions; large vessel contributions dominate when the inversion time is short whereas small vessel/perfusion will contribute significantly when the inversion time is long. With the proper inversion time and thickness of the inversion slab, predominantly mi-

crovascular-based functional maps can be obtained. Compared to the BOLD technique, FAIR functional maps are less sensitive to task-induced signal changes and artifacts.

ACKNOWLEDGMENTS

The authors thank Dr. Peter Andersen for hardware support, Gregor Adriany for construction of a quadrature birdcage coil, Dr. Frank Crosby for proofreading, and John Strupp for his processing software (STIMULATE).

REFERENCES

1. J. J. H. Ackerman, C. S. Ewy, N. N. Becker, R. A. Shalwitz, Deuterium nuclear magnetic resonance measurements of blood flow and tissue perfusion employing ^2H_2O as a freely diffusible tracer. *Proc. Natl. Acad. Sci. USA* **85,** 4099–4102 (1987).
2. S.-G. Kim, J. J. H. Ackerman, Quantitative determination of tumor blood flow via deuterium nuclear magnetic resonance spectroscopy in mice. *Cancer Res.* **48,** 3449–3453 (1988).
3. S.-G. Kim, J. J. H. Ackerman, Quantitation of regional blood flow by monitoring of exogenous tracer via nuclear magnetic resonance spectroscopy. *Magn. Reson. Med.* **14,** 266–282 (1990).
4. J. J. Neil, The validation of freely diffusible tracer methods with NMR detection for measurement of blood flow. *Magn. Reson. Med.* **19,** 299–304 (1991).
5. S.-G. Kim, J. J. H. Ackerman, Multicompartment analysis of blood flow and tissue perfusion employing D_2O as a freely diffusible tracer: a novel deuterium NMR technique demonstrated via application with murine RIF-1 tumors. *Magn. Reson. Med.* **6,** 410–426 (1988).
6. S. M. Eleff, M. D. Schnall, L. Ligetti, M. Osbakken, V. H. Subramanian, B. Chance, J. S. Leigh, Jr., Concurrent measurements of cerebral blood flow, sodium, lactate, and high energy phosphate metabolism using ^{19}F, ^{23}Na, ^1H, and ^{31}P nuclear magnetic resonance spectroscopy. *Magn. Reson. Med.* **7,** 412–424 (1988).
7. B. R. Rosen, J. W. Belliveau, H. J. Arnon, D. Kennedy, B. R. Buchbinder, A. Fischman, M. Gruber, J. Glas, R. M. Weisskoff, M. S. Cohen, F. H. Hochberg, T. J. Brady, Susceptibility contrast imaging of cerebral blood volume: human experience. *Magn. Reson. Med.* **22,** 293–299 (1991).
8. J. W. Belliveau, D. N. Kennedy, R. C. McKinstry, B. R. Buchbinder, R. M. Weissokoff, M. S. Cohen, J. M. Vevea, T. J. Brady, B. R. Rosen, Functional mapping of the human visual cortex by magnetic resonance imaging. *Science* **254,** 716–719 (1991).
9. J. A. Detre, J. S. Leigh, D. S. Williams, A. P. Koretsky, Perfusion imaging. *Magn. Reson. Med.* **23,** 37–45 (1992).
10. D. S. Williams, J. A. Detre, J. S. Leigh, A. P. Koresky, Magnetic resonance imaging of perfusion using spin inversion of arterial water. *Proc. Natl. Acad. Sci. USA* **89,** 212–216 (1992).
11. D. A. Roberts, J. A. Detre, L. Bolinger, E. K. Insko, J. S. Leigh, Quantitiative magnetic resonance imaging of human brain perfusion at 1.5 T using steady-state inversion of arterial water. *Proc. Natl. Acad. Sci. USA* **91,** 33–37 (1994).
12. R. E. Edelman, B. Siewert, D. G. Darby, V. Thangaraj, A. C. Nobre, M. M. Mesulam, S. Warach, Qualitative mapping of cerebral blood flow and functional localization with echo-planar MR imaging and signal targeting with alternating radio frequency. *Radiology* **192,** 513–520 (1994).
13. S. D. Wolff, R. S. Balaban, Magnetization transfer contrast (MTC) and tissue water proton relaxation *in vivo*. *Magn. Reson. Med.* **10,** 135–144 (1990).
14. K. K. Kwong, J. W. Belliveau, D. A. Chesler, I. E. Goldberg, R. M. Weisskoff, B. P. Poncelet, D. N. Kennedy, B. E. Hoppel, M. S. Cohen, R. Turner, H.-M. Cheng, T. J. Brady, B. R. Rosen, Dynamic magnetic resonance imaging of human brain activity during primary sensory stimulation. *Proc. Natl. Acad. Sci. USA* **89,** 5675–5679 (1992).
15. S.-G. Kim, Quantification of relative blood flow change by flow-sensitive alternating inversion recovery (FAIR) technique: application to functional mapping. *Magn. Reson. Med.* **34,** 293–301 (1995).
16. K. K. Kwong, D. A. Chesler, R. M. Weisskoff, K. M. Donahue, T. L. Davis, L. Ostergaard, T. A. Campbell, B. R. Rosen, MR perfusion studies with T_1-weighted echo planar imaging. *Magn. Reson. Med.* **34,** 878–887 (1995).
17. S. Ogawa, T.-M. Lee, A. S. Nayak, P. Glynn, Oxygenation-sensitive contrast in magnetic resonance imaging of rodent brain at high magnetic fields. *Magn. Reson. Med.* **14,** 68–78 (1990).
18. P. Herscovitch, M. E. Raichle, What is the correct value for the brain-blood partition coefficient for water? *J. Cereb. Blood Flow Metab.* **5,** 65–69 (1985).
19. G. Adriany, J. T. Vaughan, P. Andersen, H. Merkle, M. Garwood, K. Ugurbil, Comparison between head volume coils at high fields, *in* "Proc., SMRI, 3rd Annaul Meeting, 1995" p. 747.
20. S.-G. Kim, X. Hu, G. Adriany, K. Ugurbil, Fast interleaved echo-planar imaging with navigator: high resolution anatomic and functional images at 4 Tesla. *Magn. Reson. Med.* **35,** 895–902 (1996).
21. P. A. Bandettini, A. Jesmanowicz, E. C Wong, J. S. Hyde, Processing strategies for time-course data sets in functional MRI of the human brain. *Magn. Reson. Med.* **30,** 161–173 (1993).
22. S. D. Forman, J. D. Cohen, M. Fitzgerald, W. F. Eddy, M. A. Mintun, D. C. Noll, Improved assessment of significant activation in functional magnetic resonance imaging (fMRI): use of a cluster-size threshold. *Magn. Reson. Med.* **3,** 636–647 (1995).
23. S.-G. Kim, X. Hu, K. Ugurbil, Accurate T_1 determination from inversion recovery images: application to human brain at 4 Tesla. *Magn. Reson. Med.* **31,** 445–449 (1994).
24. S.-G. Kim, J. Ashe, A. Georgopoulos, H. Merkle, J. M. Ellermann, R. S. Menon, S. Ogawa, K. Ugurbil, Functional imaging of human motor cortex at high magnetic field. *J. Neurophyiol.* **69,** 297–302 (1993).
25. S.-G. Kim, J. Ashe, K. Hendrich, J. M. Ellermann, H. Merkle, K. Ugurbil, A. Georgopoulos, Functional magnetic resonance imaging of motor cortex: hemispheric asymmetry and handedness. *Science* **261,** 615–617 (1993).
26. P. Pantano, J.-C. Baron, P. Lebrun-Grandie, N. Duquesnoy, M.-G. Bousser, D. Comar, Regional cerebral blood flow and oxygen consumption in human aging. *Stroke,* **15,** 635–641 (1984).
27. G .L. Lenzi, R. S. J. Frackowiak, T. Jones, J. D. Heather, A. A. Lammertsma, C. G. Rhodes, C. Pozzilli, $CMRO_2$ and CBF by the oxygen-15 inhalation technique. *Eur. Neurol.* **20,** 285–290 (1981).
28. D. Le Bihan, E. Breton, D. Lallemand, M. L. Aubin, J. Vignaud, M. Laval-Jeantet, Separation of diffusion and perfusion in intravoxel incoherent motion MR imaging. *Radiology* **168,** 497–505 (1988).
29. H. van As, T. J. Schaaffsma, Flow in nuclear magnetic resonance imaging, *in* "Introduction to Biomedical Nuclear Resonance" (S.B. Petersen, R.N. Muller, P.A. Rinck, Eds.), Ch. 11, pp. 68–95, Georg Theme Verlag Thieme, New York, 1985.
30. K. C. Hodde, *in* "The Cerebral Veins: An Experimental and Clinical Update" (C. M. Aver, F. Loew, Eds), pp. 85–92, Academic Press, New York, 1987.
31. W. Zhang, D. S. Williams, J. A. Detre, A. P. Koresky, Measurement of brain perfusion by volume-localized NMR spectroscopy using inversion of arterial water spins: accounting for transit time and cross-relaxation. *Magn. Reson. Med.* **25,** 362–371 (1992).
32. R. S. Menon, S. Ogawa, D. W. Tank, K. Ugurbil, 4 Tesla gradient recalled echo characteristic of photic stimulation-induced signal changes in the human primary visual cortex. *Magn. Reson. Med.* **30,** 380–386 (1993).
33. S. Lai, A. L. Hopkins, E. M. Haacke, D. Li, B. A. Wasserman, P. Buckley, L. Friedman, H. Meltzer, P. Hedera, R. Friedland, Identification of vascular structures as a major source of signal contrast in high resolution 2D and 3D functional activation imaging of the motor cortex at 1.5T: preliminary results. *Magn. Reson. Med.,* **30,** 387–392 (1993).
34. S.-G. Kim, K. Hendrich, X. Hu, H. Merkle and K. Ugurbil, Potential pitfalls of functional MRI using conventional gradient-recalled echo techniques. *NMR Biomed.* **7,** 69–74 (1994).
35. J. H. Duyn, C. T. W. Moonen, G. H. van Yperen, R. W. de Boer, P. R. Luyten, Inflow versus deoxyhemoglobin effects in BOLD functional MRI using gradient echoes at 1.5T. *NMR Biomed.* **7,** 4–9 (1994).
36. J. Frahm, K.-D. Merboldt, W. Hanicke, A. Kleinschmidt, H. Boecker, Brain and vein—oxygenation or flow? On signal physiology in functional MRI of human brain activation. *NMR Biomed.* **7,** 45–53 (1994).
37. S. Segebarth, V. Belle, C. Delon, R. Massarelli, J. Decety, J.-F. Le Bas, M. Decorps, A. L. Benabid, Functional MRI of the human brain: predominance of signals from extracerebral veins. *Neuroreport* **5,** 813–816 (1994).
38. P. E. Roland, B. Larsen, N. A. Larsen, E. Skinoj, Supplementary motor area and other cortical areas in organization of voluntary movements in man. *J. Neurophysiol.* **43,** 118–136 (1980).

39. D. J. Seitz, P. E. Roland, Learning of sequential finger movements in man: a combined kinematic and positron emission tomography (PET) study. *Eur. J. Neurosci.* **4,** 154–165 (1992).
40. S. T. Grafton, R. P. Woods, J. C. Mazziotta, M. E. Phelps, Somatotopic mapping of the primary motor cortex: activation studies with cerebral blood flow and positron emission tomography. *J. Neurophysiol.* **66,** 735–743 (1991).
41. J. G. Colebatch, M.-P. Deiber, R. E. Passingham, K. J. Friston, R. S. J. Frackowiak, Regional cerebral blood flow during voluntary arm and hand movements in human subjects. *J. Neurophysiol.* **65,** 1392–1401 (1991).
42. S. Ogawa, R. S. Menon, D. W. Tank, S.-G. Kim, H. Merkle, J. M. Ellermann, K. Ugurbil, Functional brain mapping by blood oxygenation level-dependent contrast magnetic resonance imaging. *Biophys. J.* **64,** 803–812 (1993).
43. P. E. Roland, L. Eriksson, S. Stone-Elander, L. Widen, Does mental activity change the oxidative metabolism of the brain? *J. Neurosci.* **7,** 2373–2389 (1987).
44. R. J. Seitz, P. E. Roland, Vibratory stimulation increases and decreases the regional cerebral blood flow and oxidative metabolism: a positron emission tomography (PET) study. *Acta Neurol. Scand.* **86,** 60–67 (1992).